The Journal of Experimental Biology 209, 3170-3182
Published by The Company of Biologists 2006
doi:10.1242/jeb.02369

Visual stimulation of saccades in magnetically tethered *Drosophila*

John A. Bender* and Michael H. Dickinson
Division of Biology, California Institute of Technology, Pasadena, CA 91125, USA
*Author for correspondence (e-mail: jbender@caltech.edu)

Accepted 5 June 2006

Summary

Flying fruit flies, *Drosophila melanogaster*, perform 'body saccades', in which they change heading by about 90° in roughly 70 ms. In free flight, visual expansion can evoke saccades, and saccade-like turns are triggered by similar stimuli in tethered flies. However, because the fictive turns in rigidly tethered flies follow a much longer time course, the extent to which these two behaviors share a common neural basis is unknown. A key difference between tethered and free flight conditions is the presence of additional sensory cues in the latter, which might serve to modify the time course of the saccade motor program. To study the role of sensory feedback in saccades, we have developed a new preparation in which a fly is tethered to a fine steel pin that is aligned within a vertically oriented magnetic field, allowing it to rotate freely around its yaw axis. In this experimental paradigm, flies perform rapid turns averaging 35° in 80 ms, similar to the kinematics of free flight saccades. Our results indicate that tethered and free flight saccades share a common neural basis, but that the lack of appropriate feedback signals distorts the behavior performed by rigidly fixed flies. Using our new paradigm, we also investigated the features of visual stimuli that elicit saccades. Our data suggest that saccades are triggered when expanding objects reach a critical threshold size, but that their timing depends little on the precise time course of expansion. These results are consistent with expansion detection circuits studied in other insects, but do not exclude other models based on the integration of local movement detectors.

Key words: *Drosophila*, saccade, vision.

Introduction

Many flies, including the fruit fly, *Drosophila melanogaster*, exhibit a flight pattern in which straight segments are interspersed with rapid turns called saccades (Land and Collett, 1974; Collett and Land, 1975; Egelhaaf and Kern, 2002; Schilstra and van Hateren, 1999). Land (Land, 1999) suggested that these so-called 'body' saccades might be analogous to visual saccades in humans and other primates, and noted that similar periods of stable gazing interspersed with rapid shifts have been observed across three phyla. One proposed function of visual saccades in primates is to quickly move the fovea, with its high spatial resolution but limited spatial extent, around a large visual field to process key features (after Yarbus, 1961).

Separate from the functional utility of saccades, their underlying neural basis is of interest because they represent rapid and robust responses to environmental stimuli. An analysis of free flight trajectories in different visual environments suggested that visual expansion can trigger saccades in free flight (Tammero and Dickinson, 2002a). Tethered flies exhibit saccade-like behaviors (Heisenberg and Wolf, 1979; Wolf and Heisenberg, 1980; Tammero and Dickinson, 2002b), but because these events are much longer, it is not known whether these fictive turns are analogous at the neurobiological level to free flight saccades. In an attempt to clarify this, Mayer and co-workers (Mayer et al., 1988) tethered flies to a flexible filament in such a way that the flies could rotate about their yaw axis but were otherwise fixed in space. Flies in this arrangement exhibited saccade-like behaviors, but those authors could not identify a visual stimulus sufficient to evoke them, which obscures a clear connection between the free flight behavior and its putative tethered flight counterpart. Further, fictive saccades in rigidly tethered *Drosophila* last approximately 500 ms (Heisenberg and Wolf, 1979; Tammero and Dickinson, 2002b), around ten times longer than free flight saccades (Fry et al., 2003), and the duration is nearly independent of any visual feedback. The most likely explanation for the difference in time course between saccades in free flight and in tethered flight is a role for sensory feedback in terminating the saccade motor program, but the modalities responsible for this feedback have not been identified. The halteres, the modified hindwings of flies that act as gyroscopes (Pringle, 1948; Nalbach, 1993), are a likely source, but their involvement has not been explicitly examined. In addition, whereas the torque produced during fictive saccades is unidirectional, an analysis of free flight saccades shows that flies must generate countertorque to terminate each turn (Fry et al., 2003), again suggesting an important role for sensory feedback that is not present in tethered flight.

To address the issue of whether free flight saccades and fictive turns in tethered flight share the same neurobiological foundations, we have developed a novel behavioral paradigm. We tether a fly to a steel pin placed within a magnetic field, allowing the fly to rotate freely about its yaw axis. This arrangement provides naturalistic sensory feedback from yaw rotation, which is mediated by the visual system and the halteres (Dickinson, 1999). Using this preparation, we show that the rapid turns observed under these magnetically tethered conditions are quite similar to free flight saccades and thus likely result from the same motor program. We also controlled the visual environment using an electronic panorama to directly test whether and how certain visual stimuli elicit saccades. The results show that looming objects evoke saccades with a probability independent of the object's shape. The timing of saccades relative to a virtual collision depends on the object's velocity in a manner similar to the visual threshold model proposed by Gabbiani and co-workers (Hatsopoulos et al., 1995; Gabbiani et al., 1999; Gabbiani et al., 2001) based on recordings from single neurons in locusts, but is also consistent with models based on integration of elementary movement detectors (Borst, 1990).

Materials and methods

Flies

We performed experiments on 3- to 5-day-old female fruit flies, *Drosophila melanogaster* Miegen, from a laboratory culture descended from 200 wild-caught females. We anesthetized the flies by placing them on a Peltier stage held at approximately 4°C. We then attached a stainless steel pin of 50 μm diameter (nominally 0.1 mm minutien, Fine Science Tools, North Vancouver, BC, Canada) to the fly using UV-activated cement (Duro, Düsseldorf, Germany). The blunt end of the pin was fixed to the anterior of the notum with the sharp end projecting dorsally and slightly anteriorly such that when the pin was held vertically, the fly was in a hovering flight posture with a pitch angle of about 30° inclination from the horizontal (Fig. 1B). We allowed the flies to recover from anesthesia for at least 1 h before placing them in the flight arena, where they flew for 10–120 min. Any fly that did not maintain flight for at least 10 min was excluded from analysis. The data presented here come from 17.3 h of total flight by 35 flies.

Flight arena

The steel pin with the fly attached was held in the magnetic field between two vertically aligned rare earth (NdFeB) magnets (K&J Magnetics, Jamison, PA, USA) (Fig. 1A,B). The sharp end of the pin was placed in a tiny V-aperture jewel bearing (Small Parts, Miami Lakes, FL, USA) glued to the center of the upper magnet to standardize positioning and reduce rotational friction. Thus, the fly could rotate freely about the axis parallel to the magnetic field lines – its functional yaw axis. The moment of inertia of the pin about this rotational axis was 10^{-15} Nm s^2, which is less than 1% of the estimated moment of inertia of the fly (Fry et al., 2003; Mayer et al., 1988). The fly was illuminated from below with a circular array of 940 nm light-emitting diodes (LEDs), and a mirror was fixed underneath the fly to reflect an orthogonal view of the fly's ventral side to a near-IR-sensitive digital camera (A602f, Basler, Ahrensburg, Germany) running at 101 frames s^{-1}.

This arrangement of fly, magnets, light source and mirror resided within a cylindrical arena composed of 32×64 green

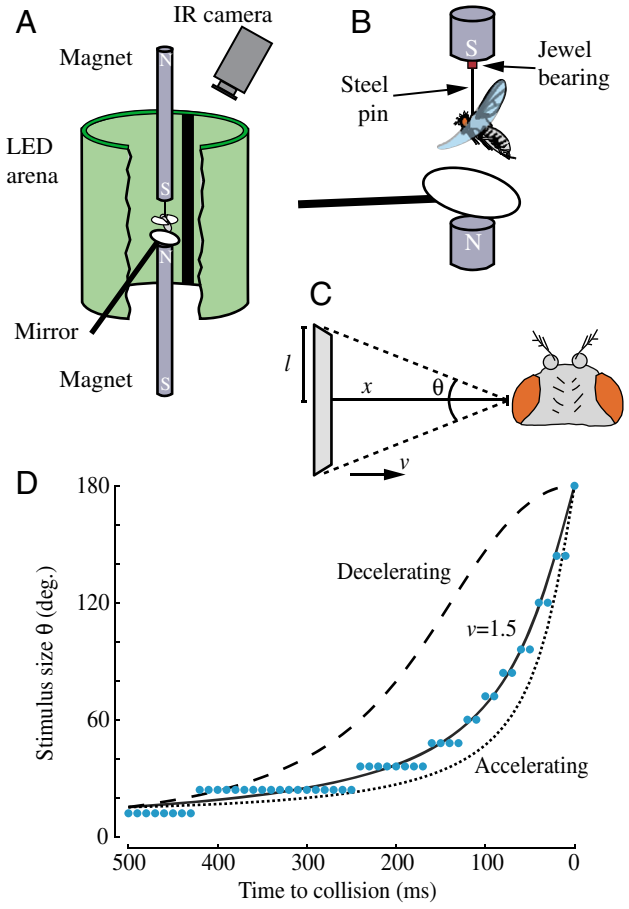

Fig. 1. Experimental design. (A) Fly orientation was determined at 101 Hz with a near-IR camera and realtime software. Visual stimulation was provided by a 32×64 matrix of LEDs wrapped in a cylinder around the tethered fly. N, magnetic north; S, south. (B) Flies were glued to a steel pin, which was set in a jewel bearing and held in a magnetic field so that the flies could rotate only about their functional yaw axis. (C) Flies were stimulated with virtual looming squares. The time course of the visual stimulus (θ) was proportional to x, the distance between the stimulus and the eye, which was determined by the square's edge half-length (l=10 cm), approach velocity v, and acceleration. (D) Time course of visual stimulation for an approaching object with constant velocity (v=1.5 m s^{-1}, solid line), acceleration (v_{init}=0, a=6.2 m s^{-2}, dotted line), or deceleration (v_{init}=3.4 m s^{-1}, a=–5.3 m s^{-2}, broken line). The stimuli were discretized both spatially and temporally due to limitations of the LED arena (visual refresh rate: 800 Hz; pattern update rate: 50 Hz). The blue circles represent the approximate discretization of the constant-velocity stimulus, sampled every 10 ms.

LEDs. Each LED subtended approximately 5.6° in the horizontal plane, and the interior of the arena had a total diameter of 8 cm and a height of 13 cm. The LED arena and associated control board were as described by M. B. Reiser and M. H. Dickinson (manuscript in preparation), except that the visual display instructions emanated directly from a computer with no bias or correction by the control board. The pattern was updated at 50 Hz, but was refreshed on the LED array at 800 Hz. The visual arena provided only a coarse spatiotemporal simulation of expansion, since *Drosophila*'s flicker-fusion rate is probably around 200 Hz (Autrum, 1958; Laughlin and Weckstrom, 1993) and the interommatidial angle is 4.6° (Götz, 1964). This is a potential area of concern, but two main lines of reasoning suggest the sufficiency of our stimulating apparatus for the purposes presented here. First, locust single neurons showed no differences in responses to looming stimuli presented using varying video refresh rates down to 67 Hz (Gabbiani et al., 1999). Second, even if our stimuli are suboptimal, they do evoke behavioral responses that discriminate between similar stimuli (see Results).

Data collection and calibration

We fine-tuned the digital processing of the images from the camera for each fly before each experiment to produce a nearly binarized image of a white fly on a black background. The center of the fly's outline in the camera image and the fly's orientation in each frame were saved for later analysis. A potential source of noise in our data lies with our ability to precisely determine the fly's orientation by this method. We estimated this error by tracking a dead fly for 1 h. The standard deviation of the orientation values under these conditions was in the range 1–2°; thus, we expect that the error in our measurement of the orientation of the flies during our experiments is also of this order. The moving wings of the live flies should not add significantly to this uncertainty because the shutter speed of the camera was too slow to visualize them.

At the beginning of a flight sequence, each fly was first subjected to a calibration phase to determine the fly's center of rotation in camera coordinates. This calibration period consisted of 1 min of visual stimulation by a horizontal square wave pattern with a fundamental spatial frequency of 45°. The motion of the pattern simulated a vertical pole of expansion and a pole of contraction separated by 180°. Under these conditions, flies robustly avoid the pole of expansion (Tammero et al., 2004). We rotated these poles around the arena at about 120° s^{-1}. Because the center of the fly in the camera image was offset from the fly's center of rotation, the centroid from each frame traced a circle as the fly spun on the tether. The center of this circle defined the fly's center of rotation in camera coordinates. Determination of this point allowed our online tracking software to unambiguously calculate the fly's heading with respect to the camera.

Another caveat related to tracking is that the relative position of the camera and the visual arena were slightly different from animal to animal. This occurred because the camera and arena had to be moved between experiments in order to insert and remove flies from the apparatus. We estimate this error to be on the order of ±5°, constrained by the physical size of the arena and the field of view of the camera. This places a lower bound on our ability to discriminate the orientation of the stimulus relative to that of the fly, but not the motion of the fly itself.

Visual stimulation

After the calibration period, we presented each fly with a 22.5×22.5° (4×4 pixel) dark square centered vertically at a fixed azimuthal position on a light background. The square was programmed to simulate an object with a half-size of 10 cm approaching the fly from 1 m away (Fig. 1C). We varied the parameters of this virtual object's approach to assess the effects on the fly's responses. In the first set of experiments (N=11 flies), we tested three conditions: the virtual object approached with either constant velocity, constant acceleration, or constant deceleration. Because the object started at the same virtual position in all cases, we varied its initial velocity in order to keep the trial duration constant. For the constant-velocity trials, the simulated speed of the virtual object was 1.5 m s^{-1} towards the fly; in the acceleration trials, the initial velocity was 0 and the object accelerated at 6.2 m s^{-2} towards the fly; in the deceleration trials, the object began at 3.4 m s^{-1} and accelerated at –5.3 m s^{-2} (Fig. 1D). In the second set of experiments (N=9), the object could change shape as it approached: expanding in either the horizontal or vertical dimension only, or expanding along one diagonal axis (top-left/bottom-right), but maintaining the same surface area as the horizontal or vertical expansions. These stimuli allowed us to test whether the responses were specific to motion along a particular axis. In these trials, the expansion time course was the same as in the constant velocity experiments for the first set of trials. In other words, these stimuli were identical to the full, expanding square with v=1.5 m s^{-1}, except that they were masked such that only a part of the square showed through (i.e. the square was viewed through a vertical, horizontal or diagonal slit) and are quantified in terms of this underlying square. For a third set of experiments (N=15), the object was programmed to approach at one of two fixed velocities (1.0 or 2.0 m s^{-1}), different from the velocity used in the previous experiments. In the final set of experiments, the object was not solid, but rather consisted of a series of alternately dark and light concentric squares radiating outward. The spatial frequency of the pattern across these squares was always 22.5°, and the outermost square had the same expansion time course as an object approaching at 1.5 m s^{-1}. This pattern was designed to enhance the stimulation of putative Reichardt-type motion detectors in the fly's visual system (Reichardt, 1961) while maintaining the same approach geometry as in the other experiments.

In each trial, we triggered one of the different expansion paradigms every 10 s. Once the object reached its full size (180° of azimuth and 117° of elevation; 32×32 pixels), it remained at that size for about 5 s. For the first set of experiments, the square immediately changed back to its original size at that time. In the other trials, the object

contracted back to its original size with the same time course as that with which it expanded (Fig. 4A). In all cases, the initial and final conditions of each trial were identical – the original 22.5×22.5° dark square on a light background. However, because the fly was free to rotate around its yaw axis, the square might sit at any azimuthal position relative to the fly when stimulation occurred. Within each experiment, the order of the trials was selected randomly *ad hoc*, with the restriction that two successive trials did not use the same stimulus condition.

Saccade analysis

To isolate saccadic events for further analysis, we analyzed the orientation data using custom software written in Matlab (Mathworks, Natick, MA, USA). We calculated each fly's angular velocity by using a low-pass Butterworth filter with a 25 Hz cut-off on the orientation data and applying the central difference formula to the smoothed data (Fig. 2A). Assuming that angular velocities are normally distributed during 'straight' flight and that there are a small number of saccades relative to the total flight duration, we set a threshold of four standard deviations away from the mean angular velocity of the entire data set. Whenever the angular velocity exceeded this threshold, those events were classified as saccades. We analyzed a total of 26 535 such events.

We quantified the duration of each saccade as the time interval over which the angular velocity exceeded one-quarter of its maximum value for that event. To determine the amplitude of each saccade, we used the difference of the fly's median orientations during two 50 ms windows – one window before and one after the fly's angular velocity exceeded one-quarter of its maximum value (Fig. 2B). To avoid inclusion of tracking error, we set bounds on the amplitude of the saccades used in subsequent analysis; only saccades between 15° and 150° amplitude were included.

When measuring the probability of saccade occurrence in response to a stimulus, we looked for saccades in a 500 ms window beginning 30 ms after the start of the stimulus. However, in the trials in which the object's velocity was 1.0 m s^{-1}, this brief window did not include the time of the virtual collision. For these trials, we used a 500 ms window beginning 280 ms after the beginning of the stimulus. Visual inspection of the saccade distribution over the course of the stimulus did not suggest a significantly different saccadic frequency during the initial 280 ms than during a similar period in which there was no stimulation (data not shown). If there was more than one saccade in the 500 ms window, only the first was analyzed. By these criteria, we observed a total of 2933 saccades that we assigned as having been triggered by visual expansion. To estimate the spontaneous saccade rate, we calculated the probability of a saccade occurrence in a 500 ms window beginning 3 s after a stimulus presentation.

We used a *k*-fold cross-validation technique (with k=10) to estimate saccade metrics (amplitude, duration and peak angular velocity) from various stimulation parameters. In this analysis, we divided the data randomly into 10 blocks (i.e. k=10). For each block, which represented 10% of the entire data set, we fit a second-order polynomial to the other 90% of the data and then evaluated the predictive ability of this model on the current, excluded block, using the mean-squared error (MSE) of the prediction to measure its precision. We then compared the mean of these 10 MSE measurements with the naïve MSE (the overall variance for a particular saccade metric) to

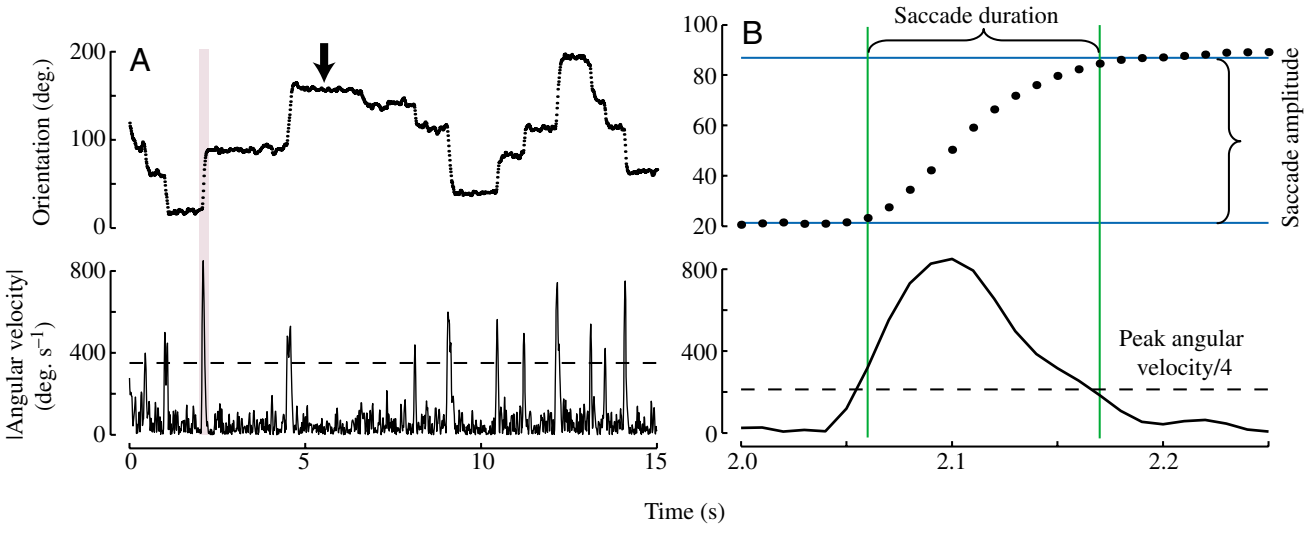

Fig. 2. Spontaneous behavior in the flight arena and methods used to quantify saccades. (A) Orientation data sampled every 10 ms (101 Hz) reveal periods of rapid turning (top). The small, slow (~0.5 Hz) oscillations (arrow) were noticeable by eye, and do not represent tracking noise. The orientation data were low-pass filtered at 25 Hz before calculating the angular velocity (bottom). The saccade threshold (broken line) was set 4 s.d. away from 0, at about 350° s^{-1}. (B) Magnification of the region within the shaded box from A, containing one saccade. Saccade duration (green lines) was the time during which the fly's angular velocity exceeded one-quarter of its peak angular velocity during that saccade (broken line). Saccade amplitude (blue lines) was the difference between the median of the 5 points before and after the saccade.

determine how much of the behavioral variation could be explained by each stimulus parameter. Although a monomial model had slightly less predictive power, increasing the order of the polynomial model beyond second-order did not improve the predictions (data not shown).

Modeling of saccade initiation

Gabbiani and co-workers (Gabbiani et al., 1999; Gabbiani et al., 2001), visually simulating objects approaching with a constant velocity, reported that the locust motion-sensitive neuron DCMD responded at its peak firing rate with a constant delay after a looming stimulus reached a fixed critical size. They note that the time course of visual stimulation in this paradigm depends only on the quantity l/v, the ratio of the object's half-size (l) and its velocity v, irrespective of whether the object is a circle or a square. Their data fit tightly to the linear relationship:

$$t_{peak} = \alpha l/v - \delta \,, \quad (1)$$

where t_{peak} was the time of the DCMD neuron's peak firing rate and δ was the delay between the time the stimulus reached critical size (t_{crit}) and t_{peak}. The coefficient α is related to the critical angle, θ_{crit}, by:

$$\theta_{crit} = 2\tan^{-1}(1/\alpha) \,. \quad (2)$$

The linear relationship between t_{peak} and l/v means that θ_{crit} is constant.

Although we used only three values of l/v with our constant-velocity stimuli, we utilized the fact that l/v varied monotonically during the accelerating and decelerating stimuli to estimate α and δ, using the peak in behavioral response probability rather than neural firing rate to determine t_{peak}. To do this, we first calculated the probability of saccade initiation as a function of post-stimulus time. We then filtered this function using a 5 Hz low-pass Butterworth filter and found its peak time, t_{peak} (Fig. 8A). Using the values of l/v at t=t_{peak} for the accelerating and decelerating stimuli and the constant values of l/v for the other square stimuli, we calculated α and δ. However, for the accelerating and decelerating stimuli, the value of l/v changed between t_{crit} and t_{peak}. Because δ represents this delay, we replaced l/v in the regression matrices with the values of l/v at t=(t_{peak}–δ) and recalculated α and δ. We performed this transformation iteratively until δ was changing by less than 0.01 ms – generally within 5–10 iterations.

Results

Observations on magnetically tethered flight

Flies tethered to steel pins with a free yaw axis perform distinct, rapid turns, which we recorded using a digital camera and computer (see Materials and methods; Fig. 2A). The distribution of the angular velocities under such conditions is well approximated by the sum of a Gaussian with a mean of –0.31° s^{-1} and a standard deviation of 87.7° s^{-1}, and an exponential with a decay constant of 0.0017° s^{-1}. This is qualitatively similar to the observations made by Mayer and co-workers (Mayer et al., 1988), who used a flexible filament to tether their flies.

We interpret this distribution as evidence of a system with two states: a noisy straight flight state and an active turning state. This is consistent with observations made in free flight (Collett and Land, 1975; Tammero and Dickinson, 2002a), where these turning events are termed 'body saccades'. We set a threshold 4 s.d. away from the mean angular velocity, at ±350° s^{-1}, to separate saccades from free flight. We calculated the duration and amplitude of saccadic events in our

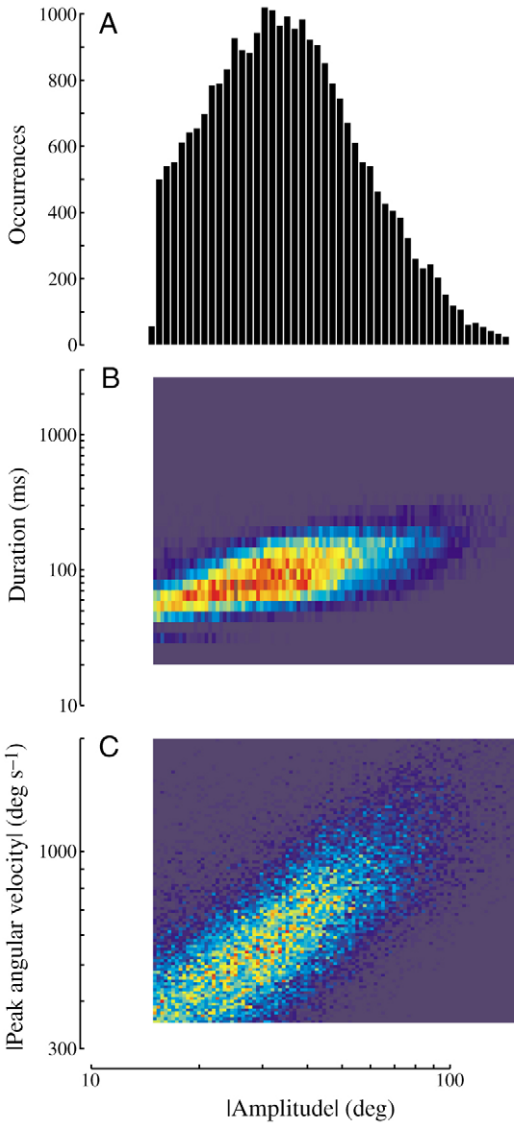

Fig. 3. Saccade amplitude, duration and peak angular velocity are correlated. (A) Histogram of absolute saccade amplitude. The mean value of the data shown in this histogram is 35.2°. Saccades with amplitudes <15° or >150° were not analyzed, since they may represent tracking errors. (B,C) 2-dimensional histograms. (B) Saccade duration, sampled at 101 Hz, loses correlation with saccade amplitude as amplitude increases. (C) Peak angular velocity during a saccade is tightly coupled to saccade amplitude. The bottom of C is truncated at the angular velocity saccade threshold. N=35 flies, n=26535 saccades.

preparation (see Materials and methods; Fig. 2B) and compared the co-distribution of those parameters with previous observations made using a filament tether (Mayer et al., 1988) (Fig. 3). Again, there is a good qualitative match between data sets (see Discussion). The amplitude, duration and peak angular velocity of these saccades are well approximated by log-normal distributions. The mean absolute amplitude using this distribution was 35.2±1.6°, the mean duration was 78.5±1.4 ms, and the mean peak absolute angular velocity was 637.8±1.4° s^{-1}. The relationship between peak velocity and amplitude is tighter than that between duration and amplitude (Fig. 3; Pearson coefficient ρ=0.59 for amplitude/duration, ρ=0.70 for amplitude/peak velocity), but duration and peak velocity are uncorrelated (ρ=0.06).

Saccade stimulation parameters

Mayer and colleagues did not identify a stimulus that elicited saccades (Mayer et al., 1988). However, recent free flight observations (Tammero and Dickinson, 2002a) and experiments using a rigid tether (Tammero and Dickinson, 2002b), suggest that visual expansion may trigger saccades. Therefore, we presented our flies with visual stimuli simulating the approach of a dark, square object (see Materials and methods; Fig. 1). Accelerating, decelerating and constant-velocity (v=1.5 m s^{-1}) stimuli all evoked saccades at a probability significantly higher than that due to the spontaneous saccade rate (ANOVA, P<0.01) (Fig. 4B).

We investigated the directional sensitivity of the visual response in separate experiments in which the square expanded only along one axis (vertical, horizontal or diagonal). For comparison, we also presented these flies with a full expansion stimulus (v=1.5 m s^{-1}). Because some prior experiments on rigidly tethered animals are ambiguous as to whether flies avoid expansion or fixate contracting stimuli (Tammero et al., 2004), the stimuli in these trials were presented as contractions as well as expansions. Halfway between expansion trials, the stimulus would contract back to a small, dark square with the reciprocal time course to that with which it expanded (Fig. 4A). Under these conditions, all expansion stimuli reliably evoked saccades (P<0.01) (Fig. 4C). In contrast, the saccade rate following stimulus contraction was not different from baseline.

A third set of flies was presented with either a square approaching at constant velocity (at either 1.0 or 2.0 m s^{-1}) or with a concentrically striped square approaching at 1.5 m s^{-1}.

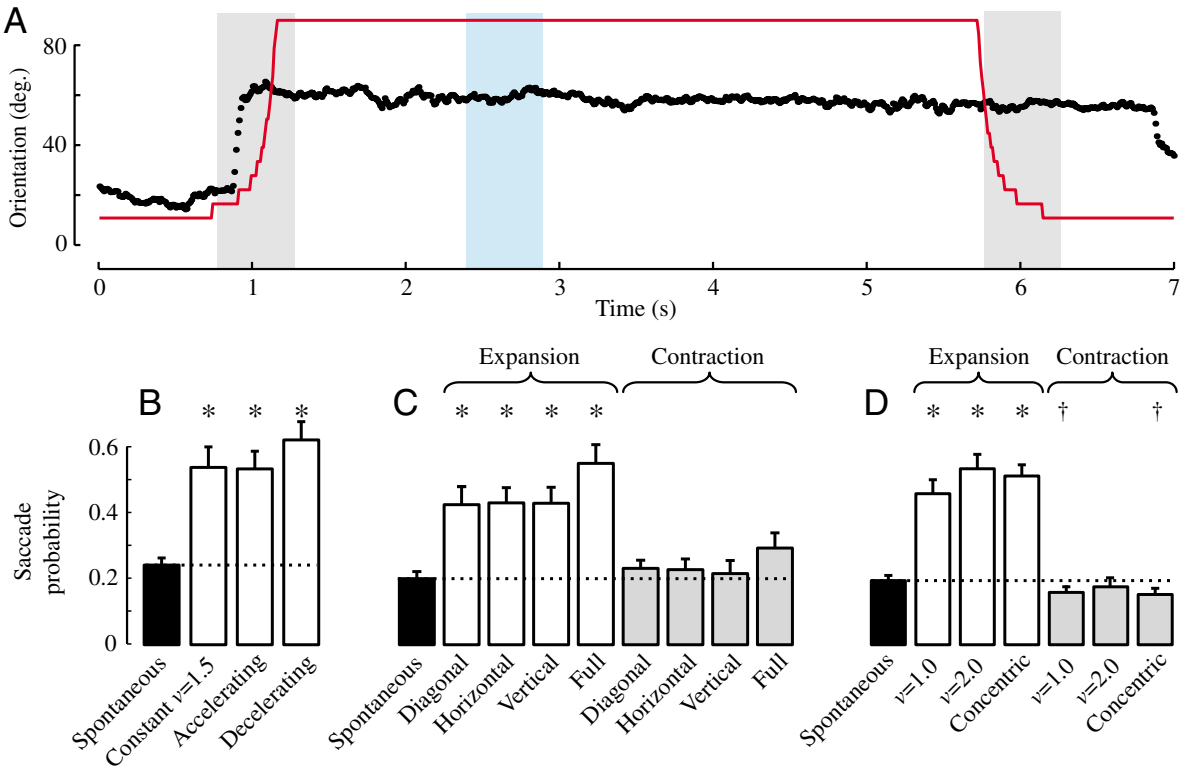

Fig. 4. Stimulus expansion evokes saccades. (A) The time course of visual stimulation (stimulus half-angle, red trace), overlaid with the fly's orientation (black dots). The gray boxes during stimulus expansion and contraction represent the 500 ms time windows during which a saccade must occur to be considered 'triggered' by the stimulus. The blue box is the time during which the spontaneous saccade rate was calculated. (B) Constant-velocity, accelerating and decelerating stimuli all elicit saccades (N=11 flies). (C) Stimuli expanding along only the horizontal, vertical or diagonal axes evoke saccades with the same probability as full-square expansion (N=9). (D) Stimuli approaching with different constant velocities have equal probability of triggering saccades. Stimuli with additional expanding edges (concentric squares) also evoke saccades at the same rate. Contraction of the low-velocity and concentric square stimuli inhibit the saccade behavior (N=15). *P<0.01; †P<0.05, relative to the spontaneous rate. Total n=2933 saccades. The error bars represent the s.e.m.; the dotted line shows the spontaneous probability.

Again, each expanding stimulus elevated the probability of observing a saccade well above baseline (P<0.01) (Fig. 4D). In this case, we observed a significantly lower saccade rate following contraction of the low-velocity square and concentric square stimuli (P<0.05), suggesting that contraction stimuli may weakly inhibit saccades under some conditions. Pairwise comparisons between the expansion-triggered saccade probabilities for all of the stimulus types did not yield any significant differences (ANOVA with Bonferroni correction for multiple comparisons, P>0.05 for each pair).

We further calculated the probability of saccade initiation as a function of time from the beginning of the stimulus (Fig. 5). The time course of stimulus expansion strongly affects the time course of saccade probability, which is consistent with results reported for rigidly tethered flies (Tammero and Dickinson, 2002b). The partial (horizontal, vertical and diagonal) stimuli elicit saccades close to the time of virtual collision (Fig. 5A–C), whereas the full square stimulus with the same expansion time course tended to evoke saccades earlier (Fig. 5D). Compared to the stimulus with v=1.5 m s^{-1} (Fig. 5D), the faster-moving stimuli are correlated with a later peak in saccade probability (Fig. 5E,H), and the slower-moving stimuli are associated with earlier saccade activity (Fig. 5F,G). The peak in saccade probability resulting from the concentric stimulus occurred earlier than that elicited by the simple square with the same time course (Fig. 5D,I). These results are difficult to reconcile with a time-to-contact avoidance response; however, a more quantitative relationship between stimulation and response timing will be discussed later.

Next, we assessed the probability of saccade initiation according to the orientation of the stimulus relative to the fly (Fig. 6Aiv). Considering all expansion stimuli together, the position of a stimulus on the fly's retina strongly affects the likelihood that the stimulus will induce a saccade. Frontal stimuli evoked saccades with higher probability than stimulation from behind. In addition, the response probability is slightly smaller for a stimulus directly in front of the fly than for a stimulus located to one side of center. A similar effect was observed for response latency in rigidly tethered flies when stimulated by square stimuli with a linear angular expansion (Tammero and Dickinson, 2002b): latency was shortest to off-center, frontal stimulation, slightly longer to frontal stimuli, and longest to rearward expansion. That study also found that the probability of the landing response, as indicated by foreleg extension, peaks in response to a frontally centered expansion stimulus. Our data are compatible with their interpretation that off-center visual expansion evokes a turning response, whereas center-symmetric expansion independently elicits a landing response and a delay or suppression of the turning response. The other statistically significant responses we found – the repression of saccades following low-velocity and concentric contraction stimuli – did not show any dependence on stimulus position (data not shown).

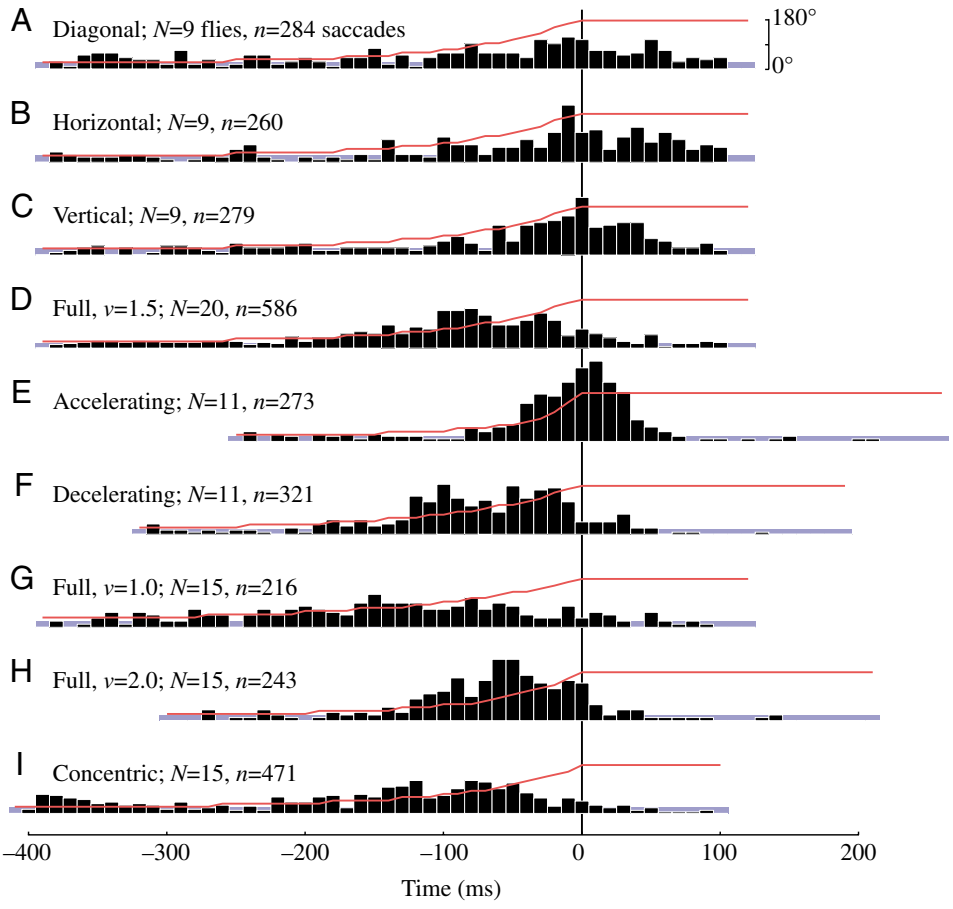

Fig. 5. The time course of stimulation affects the time course of saccade probability. (A–I) Histograms of relative saccade probability as a function of time during the 500 ms stimulation window, binned by the camera's 10 ms frame rate. The window begins 30 ms after the first discrete change in the stimulus. The red traces are the time course of stimulus size, and the blue boxes represent the spontaneous saccade rate.

Saccade dynamics

Although previous studies have shown that saccade amplitude, duration and peak velocity are correlated (Mayer et al., 1988), it is not known how stimulus parameters might affect saccade dynamics. Specifically, we estimated how stimulus position (azimuthal orientation relative to the fly), stimulus angular size, stimulus edge angular velocity, time from the start

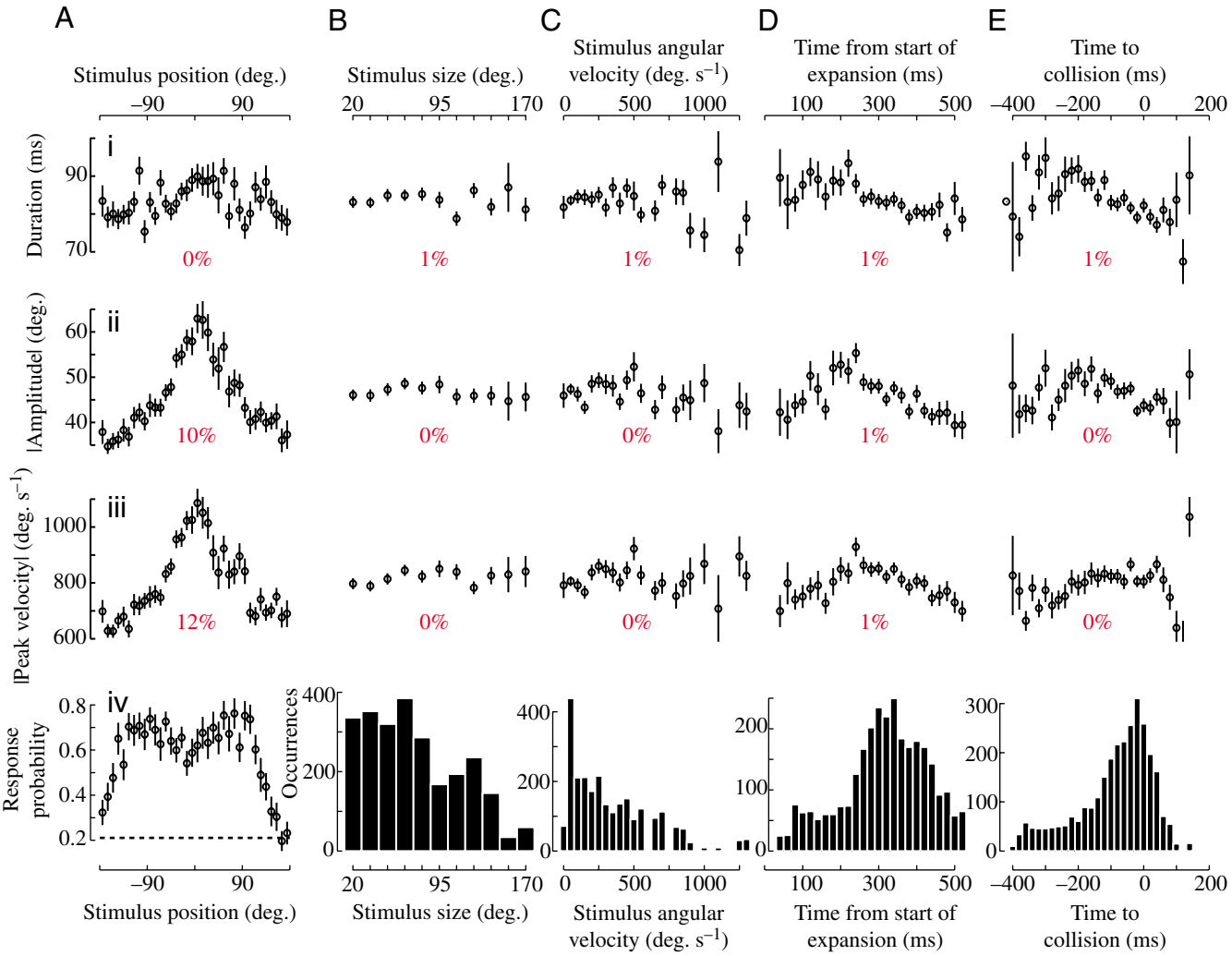

Fig. 6. Saccade metrics [rows: (i) duration, (ii) amplitude and (iii) peak velocity] are affected by stimulus parameters (columns A–E). The red numbers equal the reduction in uncertainty about the value of each metric given knowledge of that stimulus parameter. The bottom row (iv) shows the relative probability of observing each value of the stimulus parameters. The broken line in Aiv shows the spontaneous saccade probability. Values are means ± s.e.m.; *N*=35 flies; *n*=2933 saccades.

of expansion, and time to 'collision' might affect the dynamics of visually triggered saccades. Grouping all expansion stimuli together, Fig. 6i–iii shows the relationship between these factors and our three saccade metrics of choice: duration, amplitude and peak velocity.

We used *k*-fold cross-validation of a second-order polynomial model to determine the relative contributions of each factor to the final value of each metric (see Materials and methods). The only factor with any predictive value was the stimulus position relative to the fly (Fig. 6A). Saccade amplitude and peak angular velocity were largest when the stimulus was directly in front of the fly and smallest when the stimulus was behind the fly, varying smoothly in between. Knowledge of this parameter explains ~10% of the observed variance in those saccade metrics, but does not improve a prediction of saccade duration. None of the other factors tested had more than ~1% predictive value.

Discussion

We have developed an experimental paradigm in which we can present controlled visual stimuli to fruit flies that are tethered but free to rotate about their yaw axis. Using this technique, we have shown that virtual, approaching objects can evoke saccadic turns with a probability independent of object shape (Fig. 4), but that object shape and velocity do have some effect on saccade timing (Fig. 5). Furthermore, although saccades can vary somewhat in size (Fig. 3), this variation depends very little on stimulus parameters (Fig. 6). Below, we will discuss whether body saccades observed in free flight are analogous to the 'torque spikes' observed in tethered flies, and what the neurobiological basis of the saccade behavior might be.

Saccades in tethered flight

Although saccades in both freely flying and rigidly tethered *Drosophila* occur as discrete events easily discernible from

straight flight, the intersaccade trajectories in free flight are not always straight (Tammero and Dickinson, 2002a; Frye et al., 2003) [for analyses in other species, see also van Hateren and Schilstra, and Boeddeker et al. (van Hateren and Schilstra, 1999; Boeddeker et al., 2003)]. This raises the question of whether the rapid, fictive turns of tethered animals represent true saccades or gradual turns, and leaves unclear the extent to which they share similar neurobiological foundations with the free flight behaviors. It has been proposed that saccades in free flight can be triggered by visual expansion (Tammero and Dickinson, 2002a), and presentations of visual expansions to rigidly tethered flies do indeed elicit turning responses (Tammero and Dickinson, 2002b). However, these 'torque spikes' are of much longer duration than free flight saccades (Heisenberg and Wolf, 1979; Tammero and Dickinson, 2002b; Fry et al., 2003).

Consideration of body dynamics suggests that free flight saccades require the generation of torque to begin the turn and countertorque to stop (Fry et al., 2003). Rigidly tethered flies, however, never generate countertorque. Using a dynamic model, we were able to estimate the time course of torque produced by our flies during magnetically tethered saccades. The model predicts the fly's torque (τ) from the time course of its angular position (ϕ), using its moment of inertia (I) and frictional damping constant (C), by the equation $\tau=I\ddot{\phi}+C\dot{\phi}$. Fry and co-workers (Fry et al., 2003) estimated $I=5.2\times10^{-13}$ Nm s^2 and $C=5.2\times10^{-13}$ Nm s based on body morphology, but we adjusted I to compensate for the effects of tethering. The center of rotation for our flies (the tethering point) is forward of their center of mass, about which they would normally rotate. We modeled the fly as a cylinder of constant density with a moment of inertia about its center of mass approximately equal to the body morphology estimate [cylinder mass=1.25 mg, radius=0.4 mm, and length (L)=2.5 mm]. Rotating this cylinder about an axis corresponding to the tethering point (at $l=L/6$) instead of its center of mass ($l=L/2$) almost precisely doubles its moment of inertia. Using this corrected value of $I=1.0\times10^{-12}$, our model predicts a substantial countertorque phase (Fig. 7). However, it also indicates a peak torque about ten times smaller than that estimated for free flight saccades (Fry et al., 2003). There are two possible explanations for this discrepancy. First, our dynamic model may utilize inaccurate values of I and C. The value of I should be reasonably accurate, given that the fly's mass and geometry are known. The frictional coefficient is more suspect, but to explain the low torque seen here, the value would need to be 350 times larger than earlier calculations based on Stokes' Law (Fry et al., 2003), which seems unlikely even if the pin/bearing joint in our setup introduces some additional friction. Direct measurements (J. A. Bender and M. H. Dickinson, manuscript in preparation) suggest that the value of the time constant (I/C) for a magnetically tethered fly is no smaller than about 0.25 s, which bounds C at no larger than $4I$ s^{-1}.

The second, more likely explanation for the differences between our observations and those made during free flight is that the kinematics of wing motion differ between free and magnetically tethered flight. High-speed video analysis of our flies shows that they flap using a 'clap and fling' stroke (Weis-Fogh, 1973; Götz, 1987), in which the wings touch at the peak of the upstroke. These kinematics provide some additional lift (Lehmann et al., 2005) and create a large pitch moment (Fry et al., 2005), but are not normally seen in free flight (Fry et al., 2003). This suggests that, like rigidly tethered flies, magnetically tethered animals may be constantly attempting to pitch down, which could compromise their ability to create yaw torque during saccades (Lehmann and Dickinson, 2001). Furthermore, free flight saccades involve rotation around the pitch, roll and yaw axes (Schilstra and van Hateren, 1999; Fry et al., 2003), and such rotation may be important in producing the full change in heading seen in free flight. Limiting rotation about the functional pitch and roll axes would reduce the net change in heading generated by the same motor program, and thus the torque estimated by our model. We do, in fact, observe a mean saccade amplitude of 35°, instead of the 90° turns seen in free flight (Tammero and Dickinson, 2002a).

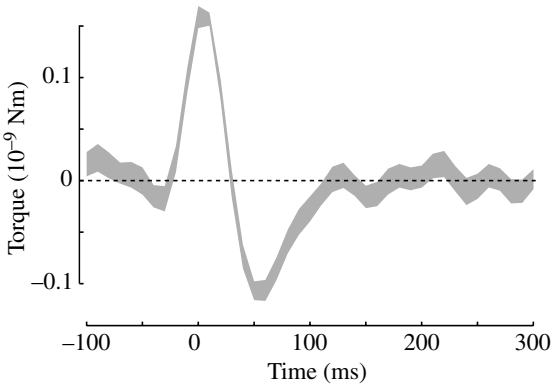

Fig. 7. The time course of torque production during a saccade by a magnetically tethered fly. Velocity and acceleration data were drawn from the saccades falling in a single bin of Fig. 3C (amplitude=17.5°, peak velocity=379° s^{-1}, n=108 saccades), rectified and aligned to the time when the angular velocity exceeded one-quarter of its maximum value. The shaded area indicates the s.e.m.

In *Drosophila*, free flight saccades have a duration of 50–70 ms (Fry et al., 2003), but the fictive behaviors in tethered flight last for 300–500 ms (Heisenberg and Wolf, 1979; Tammero and Dickinson, 2002b). One likely hypothesis that explains this difference is that although both can be evoked by similar stimuli, the termination of the saccade motor program depends on input from the halteres or other fast sensory modalities not engaged on a rigid tether. Indeed, using our magnetic tether, we observed saccade durations of 60–90 ms, quite comparable to free flight values. Earlier observations on loosely tethered flies (Heisenberg and Wolf, 1979; Mayer et al., 1988) show results qualitatively similar to ours (Fig. 3). However, for a given turn duration, the mean amplitude of turns in those experiments was smaller than in our magnetically tethered preparation. One possible explanation for these differences is that flies tethered to a filament were encumbered by more rotational friction than in our experiments – in order

to reduce torsional stiffness, Mayer and co-workers needed to use a 30 cm long, 10 μm string, which was actively spooled as the fly turned, yielding a torsion constant of 3×10^{-11} N m per revolution. In addition, they tethered their flies in a horizontal plane, while ours were inclined by 30° to better replicate free flight posture (David, 1978; Fry et al., 2003). Because saccades in free flight can involve rotations about all three body axes, the effects of restraining motion to a single plane will depend on the orientation of that plane relative to the body.

Finally, although our flight arena was designed to give the fly relatively normal feedback from the halteres about the functional yaw axis, the halteres are substantially less sensitive to yaw than to pitch and roll (Sherman and Dickinson, 2003). Therefore, it is likely that the quality of the mechanosensory feedback received by our flies during saccades is less than in free flight, yielding expected saccade dynamics somewhere in between those seen under rigidly tethered and free conditions.

In summary, we conclude that the behaviors we report here are closely related to free flight saccades, as are the fictive saccades observed in rigidly tethered flies. They are stimulated in the same way, and we find that the responses lie along a continuum correlated with the physical rotation undergone by the flies. Because the halteres serve as a gyroscope, encoding angular velocity (Pringle, 1948; Nalbach, 1993), they are a logical source for the feedback responsible for the behavioral differences. Indeed, if the neurobiological underpinnings of free flight and tethered flight saccades are the same, the only way to reconcile the differences in the time course of torque production is a role for sensory feedback in the termination of the saccade motor program.

Insights into underlying neural activity

Although previous work has shown that visual expansion can trigger saccades (Tammero and Dickinson, 2002a; Tammero and Dickinson, 2002b), it is unlikely that this is the only sensory stimulus that can do so. We observed a spontaneous saccade rate of approximately 0.4 Hz, similar to that observed by Heisenberg and Wolf in rigidly tethered *Drosophila* (Heisenberg and Wolf, 1979). In addition, there is reason to suspect that olfactory stimuli affect the rate of saccade generation both in free flight (Frye et al., 2003) and in tethered flight (Frye and Dickinson, 2004). Therefore, even if saccades are a stereotyped response, it is likely that they are elicited through multiple sensory pathways. Here, we attempt to clarify only how a subset of visual stimuli can induce saccades. Virtual objects approaching with different shapes and velocities have approximately equal probabilities of evoking saccades (Fig. 4), but the time course of stimulation affects the time course of saccade probability (Fig. 5). What, then, are the features of the stimulus that determine when a saccade is triggered?

There are two fundamentally different ways in which flies might determine when a collision is imminent. First, they could monitor the perimeter of objects in their environment, and initiate an evasive maneuver when the perimeter exceeds a certain critical value. This scheme presumes that an object has reasonably clear boundaries that can be discriminated from the visual background. Such a process would disregard information about the internal texture of an object, but show a dependency on object shape. Second, the fly could integrate motion over a large patch of visual space and initiate a saccade when the summed motion reaches some threshold. This latter process does not require that the object be distinct, with a clear boundary, but does depend on its contrast, as well as the luminance of the visual field. It further depends on the field size and time over which the local motion is integrated. While we will consider the two models separately for the moment, it is important to note that they are not mutually exclusive. It is conceivable that the fly could estimate an object's perimeter from the motion signals generated during approach. Likewise, a perimeter detection circuit with a time-varying threshold could give rise to properties similar to the motion-integration model. It was not our intention to discriminate experimentally between these two collision-avoidance models, but we will briefly discuss our results in the light of each.

Implementations of both models have been described in birds (Sun and Frost, 1998) and in insects. The motion-integration model has received much attention in fly vision literature. It is known that single cells in the lobula plate exhibit responses to pure motion (Egelhaaf et al., 1989; Borst and Egelhaaf, 1989), and specifically to some patterns of motion encountered by flying insects (Krapp and Hengstenberg, 1996; Franz and Krapp, 2000). The sensitivity of these neurons is thought to arise from the spatially integrated output of Hassenstein-Reichardt (delay-and-correlate) elementary motion detectors (EMDs) (Hassenstein and Reichardt, 1956) somewhere in the visual lobes. One behavior thought to involve EMD integration is the landing response (Borst, 1990), which is sensitive to changes in contrast, as the model predicts.

Supporting the perimeter-threshold model, however, Gabbiani and co-workers (Gabbiani et al., 1999; Hatsopoulos et al., 1995) described the response of a descending motion-sensitive neuron (DCMD) in the locust to an approaching virtual object. They found that the DCMD neuron's peak spike rate occurs with a constant delay after the stimulus reaches a critical angular size. Santer and colleagues (Santer et al., 2005) additionally demonstrated that the flying locust initiates a diving response that is correlated with the output of this neuron. Further, the time of DCMD's peak firing rate shows no dependency on stimulus texture, contrast or position (Gabbiani et al., 2001), consistent with the predictions of a perimeter detector model.

We tested the ability of the perimeter model to describe our data by using the theoretical framework developed by Gabbiani and colleagues (see Materials and methods). Briefly, their model describes the constant delay, δ, between the time the stimulus reaches a critical angle, θ_{crit}, and time of the peak spike rate in the DCMD neuron. We used the time course of saccade initiation probability (Fig. 8A) as a proxy for the spike rate of a putative DCMD homolog in *Drosophila*, with data from our solid square stimuli only (Fig. 8B, filled circles). The model predicts a linear trend, and our data fit this prediction quite well. None of the measured behavioral values differ from

the model's prediction by more than two sampling bins (of 10 ms each). We iteratively arrived at values of δ=49 ms and θ_{crit}=62° with an r^2 value of 0.91. These behavioral observations are of the same order as the range of analogous values seen in single neurons of the locust (δ=5–40 ms, θ_{crit}=15–40°, varying across individuals) (Gabbiani et al., 1999; Gabbiani et al., 2001), and the 20–30 ms delay reported in the chasing response of the house fly (Land and Collett, 1974; Collett and Land, 1975).

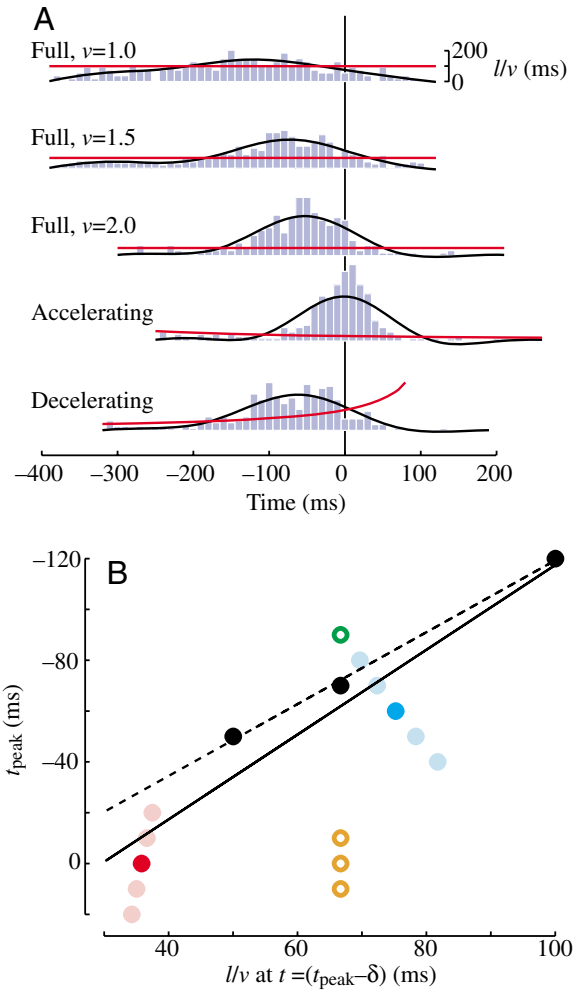

Fig. 8. Peak saccade probability occurs at a critical stimulus size regardless of the time course of stimulation. (A) The time of peak saccade probability (t_{peak}) for each stimulus was determined using a 5 Hz low-pass filter on the saccade probability histograms from Fig. 5 (not all shown here; black traces). The ratio *l*/*v* is a single metric determining the apparent size of a looming visual stimulus over time (red traces). (B) An iterative best fit to the constant-velocity (black circles), accelerating (dark red circle), and decelerating (dark blue circle) stimuli shows a strong linear relationship on this plot of t_{peak} versus *l*/*v* (regression coefficient r^2=0.91). The lighter circles behind the accelerating and decelerating stimuli show how those points would move for different values of t_{peak}; the values for the other stimuli would shift only vertically because *l*/*v* is constant. The threshold stimulus size, θ_{crit}, is derived from the slope of the black best-fit line, and equals 62° in this case. δ, the delay between the time of the critical stimulus (t_{crit}) and t_{peak}, is the *y*-intercept of this line, and evaluates to 49 ms. The orange circles are the partial (horizontal, vertical and diagonal) stimuli, and the green circle is the concentric square stimulus. The broken line was fit to the three full, constant-velocity stimuli (black circles) only (r^2=1.00). From this broken line, θ_{crit}=71° and δ=22 ms.

Because there is evidence of the existence of EMDs in the fly brain but no reported instance of a neuron directly responding to object perimeter, it is prudent to examine the predictions one might make if the angular threshold calculation were made using the spatiotemporal integration of underlying EMDs. In such a scenario, the Hassenstein-Reichardt model predicts that stimuli with concentric stripes should activate more EMDs than a uniform object would. We did, in fact, find that the time of peak saccade probability for the concentric square stimulus (Fig. 8B, green circles) was slightly earlier than that predicted by the Gabbiani model, although still within two sampling bins. Thus, our results do not provide an unambiguous answer, but the direction of the effect is the same that one would predict if the critical angle computation were, in fact, made based on EMD output. Gabbiani and co-workers (Gabbiani et al., 2001) performed this same experiment on locusts, with approximately the same result. They found a slight effect in the predicted direction (earlier peak activity), but the effect was not statistically significant. Our data also corroborate this earlier study in another way; smaller stimulus shapes with identical expansion geometry evoke later peak activity. Gabbiani and colleagues demonstrated an increased value of θ_{crit} for circular as opposed to square objects, and our data show much later saccade activity in response to our partial (horizontal, vertical and diagonal) stimuli (orange circles). The responses to these stimuli with different shapes but identical area and perimeter are indistinguishable, based on our data. Again, these effects are what one would expect if the angular threshold were calculated from EMD output. Therefore, both models might be useful in explaining our data, and there is other evidence for the existence of both in the *Drosophila* saccade system. While saccades and landing responses seem to be evoked by similar motion signals (Borst and Bahde, 1988), Tammero and Dickinson (Tammero and Dickinson, 2002b) demonstrated that the two behaviors are controlled independently. On the other hand, they also demonstrated that saccades in free flight can be explained by a large-field expansion threshold (Tammero and Dickinson, 2002a) and that rigidly tethered flies attempt to turn rapidly in response to environmental expansion even in the absence of visual 'objects' (Tammero et al., 2004).

If an angular computation is being performed by *Drosophila*, what neuron might serve as the homolog to locust DCMD? Many neurons project from the motion-sensitive visual areas of the brain to the flight control circuitry. In other dipteran insects (*Calliphora erythrocephala* and *Sarcophaga bullata*), these neurons number at least 50 pairs (Strausfeld and Gronenberg, 1990), few of which have been physiologically characterized (Gronenberg and Strausfeld, 1990). In *Drosophila*, only one pair of descending neurons – the giant descending neurons – have been studied in any detail (Levine

and Tracey, 1973; Nachtigall and Wilson, 1967; Tanouye and Wyman, 1980). Single spikes in these neurons can initiate flight (Levine, 1974; Tanouye and Wyman, 1980; Trimarchi and Schneiderman, 1995; Lima and Miesenbock, 2005), but are not thought to function during flight.

An intriguing possibility is that the haltere equilibrium system is co-opted for the purpose of saccade initiation. One function of the halteres is to sense and initiate corrections to high-frequency angular deviations (Dickinson, 1999; Sherman and Dickinson, 2003). However, since the halteres are evolutionarily modified hindwings, in addition to stroke muscles, their anatomy includes direct control muscles, similar to the steering muscles of the forewings (Bonhag, 1948; Mickoleit, 1962). Chan and colleagues (Chan et al., 1998) found that these haltere control muscles can be activated by visual input in the blowfly (*Calliphora vicina*). Therefore, perhaps saccades are initiated by efferent haltere input, using the intrinsic, reflexive counterturn response normally mediated by the halteres as an active turning mechanism. This could eliminate the necessity for a form of efference copy to be received by the halteres in order to prevent the normal, equilibrium response from counteracting a saccade command. In addition, it could provide an explanation for the high degree of stereotypy observed in saccades. Methodical manipulation of the sensory feedback received by flies during saccades is one set of experiments which would help further address the question of whether ongoing sensory feedback plays a role in modulating saccade dynamics.

List of symbols and abbreviations

C	frictional damping constant
DCMD	descending contralateral movement detector (locust)
EMD	elementary motion detector
I	moment of inertia
IR	infrared
l	stimulus half-size
L	length
LED	light-emitting diode
MSE	mean-squared error
t_{crit}	time of critical stimulus size
t_{peak}	time of peak activity
UV	ultraviolet
v	velocity
α	slope of regression line; proportional to θ_{crit}
δ	intercept of regression line; equal to a time delay
ϕ	orientation
θ_{crit}	critical angle
τ	torque

The authors gratefully acknowledge M. Reiser and Dr A. Straw for helpful comments on this analysis, and for technical assistance on stimulation and data collection, respectively. G. Card provided aid in the collection and analysis of high-speed video. This work was supported by the Institute for Collaborative Biotechnologies through grant DAAD19-03-D-0004 from the US Army Research Office.

References

Autrum, H. (1958). Electrophysiological analysis of the visual systems in insects. *Exp. Cell Res. Suppl.* **14**, 426-439.

Boeddeker, N., Kern, R. and Egelhaaf, M. (2003). Chasing a dummy target: smooth pursuit and velocity control in male blowflies. *Proc. R. Soc. Lond. B Biol. Sci.* **270**, 393-399.

Bonhag, P. F. (1948). The thoracic mechanism of the adult horsefly (Diptera: Tabanidae). *Cornell Univ. Agr. Experiment Station Memoirs* **285**, 3-39.

Borst, A. (1990). How do flies land? *Bioscience* **40**, 292-299.

Borst, A. and Bahde, S. (1988). Visual information-processing in the fly's landing system. *J. Comp. Physiol. A* **163**, 167-173.

Borst, A. and Egelhaaf, M. (1989). Principles of visual-motion detection. *Trends Neurosci.* **12**, 297-306.

Chan, W. P., Prete, F. and Dickinson, M. H. (1998). Visual input to the efferent control system of a fly's 'gyroscope'. *Science* **280**, 289-292.

Collett, T. S. and Land, M. F. (1975). Visual control of flight behavior in hoverfly, *Syritta pipiens* L. *J. Comp. Physiol.* **99**, 1-66.

David, C. T. (1978). Relationship between body angle and flight speed in free-flying *Drosophila*. *Physiol. Entomol.* **3**, 191-195.

Dickinson, M. H. (1999). Haltere-mediated equilibrium reflexes of the fruit fly, *Drosophila melanogaster*. *Philos. Trans. R. Soc. Lond. B Biol. Sci.* **354**, 903-916.

Egelhaaf, M. and Kern, R. (2002). Vision in flying insects. *Curr. Opin. Neurobiol.* **12**, 699-706.

Egelhaaf, M., Borst, A. and Reichardt, W. (1989). The nonlinear mechanism of direction selectivity in the fly motion detection system. *Naturwissenschaften* **76**, 32-35.

Franz, M. O. and Krapp, H. G. (2000). Wide-field, motion-sensitive neurons and matched filters for optic flow fields. *Biol. Cybern.* **83**, 185-197.

Fry, S. N., Sayaman, R. and Dickinson, M. H. (2003). The aerodynamics of free-flight maneuvers in *Drosophila*. *Science* **300**, 495-498.

Fry, S. N., Sayaman, R. and Dickinson, M. H. (2005). The aerodynamics of hovering flight in *Drosophila*. *J. Exp. Biol.* **208**, 2303-2318.

Frye, M. A. and Dickinson, M. H. (2004). Motor output reflects the linear superposition of visual and olfactory inputs in *Drosophila*. *J. Exp. Biol.* **207**, 123-131.

Frye, M. A., Tarsitano, M. and Dickinson, M. H. (2003). Odor localization requires visual feedback during free flight in *Drosophila melanogaster*. *J. Exp. Biol.* **206**, 843-855.

Gabbiani, F., Krapp, H. G. and Laurent, G. (1999). Computation of object approach by a wide-field, motion-sensitive neuron. *J. Neurosci.* **19**, 1122-1141.

Gabbiani, F., Mo, C. H. and Laurent, G. (2001). Invariance of angular threshold computation in a wide-field looming-sensitive neuron. *J. Neurosci.* **21**, 314-329.

Götz, K. G. (1964). Optomotorische untersuchung des visuellen systems einiger augenmutanten der fruchtfliege Drosophila. *Kybernetik* **2**, 77-92.

Götz, K. G. (1987). Course-control, metabolism and wing interference during ultralong tethered flight in *Drosophila melanogaster*. *J. Exp. Biol.* **128**, 35-46.

Gronenberg, W. and Strausfeld, N. J. (1990). Descending neurons supplying the neck and flight motor of diptera – physiological and anatomical characteristics. *J. Comp. Neurol.* **302**, 973-991.

Hassenstein, B. and Reichardt, W. (1956). Systemtheoretische analyse der zeit, reihenfolgen und vorzeichenauswertung bei der bewegungsperzeption des russelkafers chlorophanus. *Z. Naturforsch. B Chem. Biochem. Biophys. Biol. Verwandten Geb.* **11**, 513-524.

Hatsopoulos, N., Gabbiani, F. and Laurent, G. (1995). Elementary computation of object approach by a wide-field visual neuron. *Science* **270**, 1000-1003.

Heisenberg, M. and Wolf, R. (1979). On the fine-structure of yaw torque in visual flight orientation of *Drosophila melanogaster. J. Comp. Physiol.* **130**, 113-130.

Krapp, H. G. and Hengstenberg, R. (1996). Estimation of self-motion by optic flow processing in single visual interneurons. *Nature* **384**, 463-466.

Land, M. F. (1999). Motion and vision: why animals move their eyes. *J. Comp. Physiol. A* **185**, 341-352.

Land, M. F. and Collett, T. S. (1974). Chasing behavior of houseflies (Fannia-Canicularis) – description and analysis. *J. Comp. Physiol.* **89**, 331-357.

Laughlin, S. B. and Weckstrom, M. (1993). Fast and slow photoreceptors – a comparative-study of the functional diversity of coding and conductances in the diptera. *J. Comp. Physiol. A* **172**, 593-609.

Lehmann, F. O. and Dickinson, M. H. (2001). The production of elevated flight force compromises manoeuvrability in the fruit fly *Drosophila melanogaster*. *J. Exp. Biol.* **204**, 627-635.

Lehmann, F. O., Sane, S. P. and Dickinson, M. (2005). The aerodynamic effects of wing–wing interaction in flapping insect wings. *J. Exp. Biol.* **208**, 3075-3092.

Levine, J. and Tracey, D. (1973). Structure and function of giant motorneuron of *Drosophila melanogaster*. *J. Comp. Physiol.* **87**, 213-235.

Levine, J. D. (1974). Giant neuron input in mutant and wild-type *Drosophila*. *J. Comp. Physiol.* **93**, 265-285.

Lima, S. Q. and Miesenbock, G. (2005). Remote control of behavior through genetically targeted photostimulation of neurons. *Cell* **121**, 141-152.

Mayer, M., Vogtmann, K., Bausenwein, B., Wolf, R. and Heisenberg, M. (1988). Flight control during free yaw turns in *Drosophila melanogaster*. *J. Comp. Physiol. A* **163**, 389-399.

Mickoleit, G. (1962). Die thoraxmuskulatur von tipula vernalis meigen. ein beitrag zur vergleichenden anatomie des dipteranthorax. *Zool. Jahrb. Abt. Anat. Ontogenie Tiere* **80**, 213-244.

Nachtigall, W. and Wilson, D. M. (1967). Neuro-muscular control of dipteran flight. *J. Exp. Biol.* **47**, 77-97.

Nalbach, G. (1993). The halteres of the blowfly Calliphora. 1. Kinematics and dynamics. *J. Comp. Physiol. A* **173**, 293-300.

Pringle, J. W. S. (1948). The gyroscopic mechanism of the halteres of diptera. *Philos. Trans. R. Soc. Lond. B Biol. Sci.* **233**, 347-384.

Reichardt, W. (1961). Autocorrelation, a principle for relative movement discrimination by the central nervous system. In *Sensory Communication* (ed. W. Rosenblith), pp. 303-317. New York: MIT Press.

Santer, R. D., Simmons, P. J. and Rind, F. C. (2005). Gliding behaviour elicited by lateral looming stimuli in flying locusts. *J. Comp. Physiol. A* **191**, 61-73.

Schilstra, C. and van Hateren, J. H. (1999). Blowfly flight and optic flow. I. Thorax kinematics and flight dynamics. *J. Exp. Biol.* **202**, 1481-1490.

Sherman, A. and Dickinson, M. H. (2003). A comparison of visual and haltere-mediated equilibrium reflexes in the fruit fly *Drosophila melanogaster*. *J. Exp. Biol.* **206**, 295-302.

Strausfeld, N. J. and Gronenberg, W. (1990). Descending neurons supplying the neck and flight motor of diptera – organization and neuroanatomical relationships with visual pathways. *J. Comp. Neurol.* **302**, 954-972.

Sun, H. J. and Frost, B. J. (1998). Computation of different optical variables of looming objects in pigeon nucleus rotundus neurons. *Nat. Neurosci.* **1**, 296-303.

Tammero, L. F. and Dickinson, M. H. (2002a). The influence of visual landscape on the free flight behavior of the fruit fly *Drosophila melanogaster*. *J. Exp. Biol.* **205**, 327-343.

Tammero, L. F. and Dickinson, M. H. (2002b). Collision-avoidance and landing responses are mediated by separate pathways in the fruit fly, *Drosophila melanogaster*. *J. Exp. Biol.* **205**, 2785-2798.

Tammero, L. F., Frye, M. A. and Dickinson, M. H. (2004). Spatial organization of visuomotor reflexes in *Drosophila*. *J. Exp. Biol.* **207**, 113-122.

Tanouye, M. A. and Wyman, R. J. (1980). Motor outputs of giant nerve-fiber in *Drosophila*. *J. Neurophysiol.* **44**, 405-421.

Trimarchi, J. R. and Schneiderman, A. M. (1995). Flight initiations in Drosophila-melanogaster are mediated by several distinct motor patterns. *J. Comp. Physiol. A* **176**, 355-364.

van Hateren, J. H. and Schilstra, C. (1999). Blowfly flight and optic flow. II. Head movements during flight. *J. Exp. Biol.* **202**, 1491-1500.

Weis-Fogh, T. (1973). Quick estimates of flight fitness in hovering animals, including novel mechanisms for lift production. *J. Exp. Biol.* **59**, 169-230.

Wolf, R. and Heisenberg, M. (1980). On the fine-structure of yaw torque in visual flight orientation of *Drosophila melanogaster*. 2. A temporally and spatially variable weighting function for the visual-field (visual-attention). *J. Comp. Physiol.* **140**, 69-80.

Yarbus, A. L. (1961). Eye movements during examination of complicated objects. *Biofizika* **6**, 52-56.